

Synchronized Aharonov-Bohm Motifs via Engineered Dissipation

Christopher W. Wächtler^{1,*} and Gloria Platero¹

¹*Instituto de Ciencia de Materiales de Madrid ICMN-CSIC, Madrid 28049, Spain*

(Dated: November 25, 2025)

The interplay between external gauge fields and lattice geometry can induce extreme localization dynamics through complete destructive interference. We show that combining this flux-induced localization with engineered dissipation leads to robust spin synchronization in rotationally symmetric spin geometries, referred to as Aharonov–Bohm motifs, with cyclic symmetries of any order. The synchronized dynamics is independent of initial conditions and features entanglement among spins within each motif. We further demonstrate that multiple motifs can fully synchronize when coupled, which is achieved by applying additional collective dissipation acting on all intra-motif spins. These results reveal a direct connection between flux-induced localization, dissipative engineering, and collective quantum synchronization.

Introduction.—Gauge field fluxes fundamentally influence the dynamics of quantum particles and give rise to many intriguing phenomena in condensed matter physics, such as the integer and fractional quantum Hall effects [1–3]. Recent experimental advances of realizing synthetic gauge fields in engineered quantum platforms, including neutral atoms [4–7], superconducting circuits [8, 9] and trapped ions [10, 11], have opened new possibilities for realizing and probing flux-induced effects in a highly controlled way. A prominent example is Aharonov–Bohm (AB) caging [12], which appears in lattice models where gauge potentials impose direction-dependent phases that interfere destructively and thereby convert extended Bloch waves into compact localized states, giving rise to perfectly flat (dispersionless) bands in extended lattices. AB caging occurs in a variety of geometries, including rhombic chains [13–15], Creutz ladders [16, 17], and the two-dimensional dice lattices [12], all of which exhibit complete flux-induced destructive interference at π -flux (i.e. half a flux quantum) per plaquette. Since its initial discovery in conducting wires [18, 19], AB caging has been realized in a variety of other platforms, including photonic lattices [20, 21], ultracold atoms [22, 23], and superconducting qubits [24].

Dissipation and decoherence are traditionally regarded as detrimental to coherence-driven phenomena such as AB caging [22]. However, when engineered properly and used strategically, dissipation can also act as a resource, for example to prepare nontrivial states [25–27] or to induce nonequilibrium phases and phase transitions [28–33]. A prominent example of the interplay between coherent and dissipative dynamics is quantum synchronization [34–44]. Over the past decade, this field has progressed rapidly, with the first experimental realizations probing how classical nonlinear behavior manifests in the quantum regime [45–49], and identifying intrinsically quantum aspects of synchronization, in particular its connection to entanglement [50–53] and quantum interference [54, 55]. More recently, the emergence of synchronized dynamics in condensed-matter and many-body settings has attracted growing attention [52, 56, 57], giv-

ing rise to concepts such as topological quantum synchronization [43, 58].

In this Letter, we identify a mechanism by which synthetic gauge fields and engineered dissipation cooperate to produce synchronized spin dynamics in two-dimensional spin motifs. Specifically, we show that local dissipation in rotationally symmetric motifs with \mathcal{C}_n -symmetry (with $n \geq 2$ the order of rotation) induces synchronization of the magnetization (i.e. $\langle \sigma^z(t) \rangle$), with dynamics reminiscent of AB caging but notably more robust: almost all initial conditions evolve into synchronized motion in stark contrast to the dynamics without dissipation. We prove that this mechanism is universal to all \mathcal{C}_n -symmetric geometries, which we term Aharonov–Bohm motifs, and derive analytic solutions describing both the dissipative dynamics and the evolution of entanglement, expressed through the concurrence. Furthermore, we demonstrate that synchronization extends beyond individual motifs: inter-motif couplings and collective dissipation channels can fully align the dynamics across interacting AB motifs. Our results have twofold implications: on the condensed-matter side, they establish engineered dissipation as a means to realize correlated dynamics with potential future applications in interference-based flat-band systems [17, 59, 60]; on the synchronization side, they reveal a previously unrecognized connection between synchronization and (synthetic) gauge fields, which opens up new avenues for exploring collective quantum behavior.

Dissipative Aharonov–Bohm Motifs.—We consider a system of interacting spins arranged in plaquettes of four spins. Several plaquettes are connected so that the resulting structure has a \mathcal{C}_n -rotational symmetry, where n is the number of plaquettes meeting at a common central spin; examples of motifs with different cyclic order n are shown in the insets of Figs. 1a–c. The total number of spins in a \mathcal{C}_n -symmetric motif is therefore $N = 2n + 1$. A synthetic gauge flux ϕ threads the plaquettes of the motifs. Such fluxes in spin systems can be implemented experimentally in various platforms, including superconducting qubits and trapped ions [10, 61–63]. The coher-

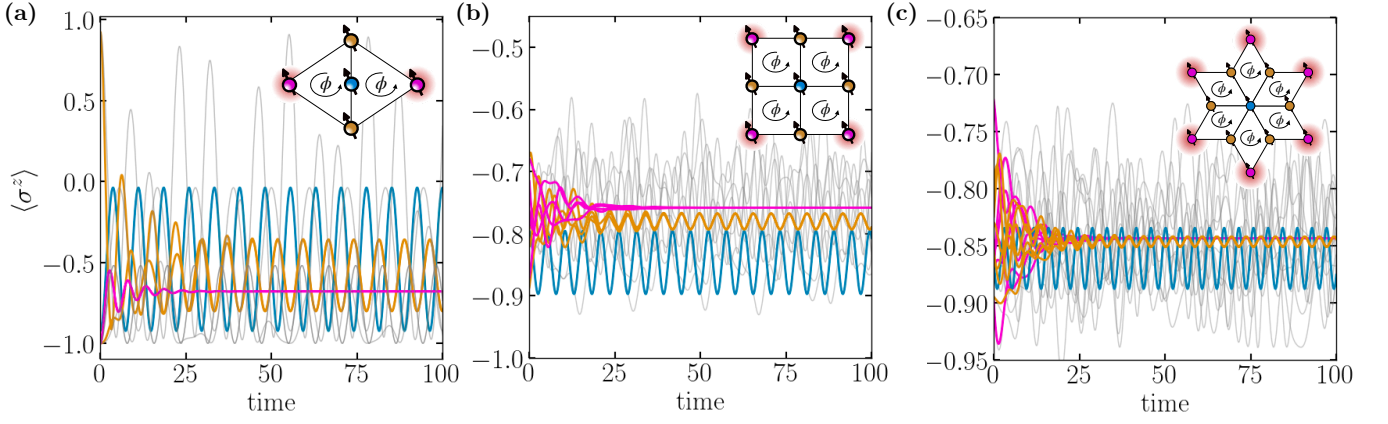


Figure 1. Synchronized dynamics in spin motifs of different cyclic order \mathcal{C}_n arising from the cooperative interplay between AB interference and locally applied dissipation. (a) Motif of order $n = 2$ with $N = 5$ spins, (b) motif of order $n = 4$ with $N = 9$ spins, and (c) motif of order $n = 6$ with $N = 13$ spins. Each motif consists of n plaquettes corresponding to the cyclic order \mathcal{C}_n . When a gauge flux $\phi = \pi$ threads each plaquette and dissipation acts on the outer (pink) spins (indicated by the red discs), the local magnetization $\langle \sigma_\alpha^z(t) \rangle$ of the inner (brown) spins becomes synchronized with each other and anti-synchronized with the central (blue) spin. The gray background lines show the corresponding dynamics in the absence of dissipation, starting from the same random initial conditions. Parameters: $h = 1.0$, $g = 0.3$, $\phi = \pi$, $\gamma = 0.1$.

ent dynamics of the N spins is governed by the Hamiltonian

$$H_n = h \left(\sigma_c^z + \sum_{i=1}^n [\sigma_i^z + \sigma_{i,i+1}^z] \right) + g \sum_{i=1}^n (e^{i\phi_i} \sigma_c^+ \sigma_i^- + e^{i\phi_{i,i+1}} \sigma_i^+ \sigma_{i,i+1}^- + \text{h.c.}), \quad (1)$$

where σ_α^z are the Pauli- z operators and $\sigma_\alpha^\pm = (\sigma_\alpha^x \pm i \sigma_\alpha^y)/2$ are the usual raising and lowering operators. The parameters $h > 0$ and $g > 0$ denote the on-site field strength and the interaction amplitude, respectively. The indices in Eq. (1) are defined as follows: the central spin is labeled c ; the *inner* spins, each coupled directly to the central spin, are labeled by a single index $i \in \{1, \dots, n\}$; and the *outer* spins, which connect neighboring inner spins and close the plaquettes, are labeled by a double index $(i, i+1)$. A periodic boundary conditions is implied for the indices, i.e., $n+1 \equiv 1$. Each plaquette is therefore formed by the four spins $[c, i, (i, i+1), i+1]$. The total flux threading each plaquette is given by $\phi = \sum_{\square} \phi_\alpha$, where the local phases ϕ_α (with α a single or double index) are defined up to a gauge freedom. Throughout, we set $\phi = \pi$ unless otherwise specified.

In addition to the coherent dynamics, we introduce local dissipation acting on the outer spins with index $(i, i+1)$ of each motif. The resulting dissipative dynamics is described by a Lindblad master equation for the system density matrix $\dot{\rho} = \mathcal{L}[\rho]$ with the Liouvillian defined as

$$\mathcal{L}[\rho(t)] = -i[H_n, \rho(t)] + \sum_{i=1}^n \gamma \mathcal{D}[\sigma_{i,i+1}^z] \rho, \quad (2)$$

where $\mathcal{D}[O]\rho = O\rho O^\dagger - \frac{1}{2}\{O^\dagger O, \rho\}$ and γ denotes a dissipation rate assumed identical for all spins for simplicity. Such local dissipation may be realized via repeatedly measuring (or replacing) ancillary spins [49, 64]

Solving the full open-system dynamics becomes numerically demanding for motifs with large n . However, the total magnetization $M = \sum_\alpha \sigma_\alpha^z$ is conserved by the Hamiltonian, $[H_n, M] = 0$, and also commutes with all Lindblad operators, $[\sigma_{i,i+1}^z, M] = 0$. The dynamics therefore decomposes into independent magnetization sectors labeled by $m \in \{-N, -N+2, \dots, N\}$. As shown in the Supplementary Material [65], all sectors except the single-magnon subspaces with $m = \pm(N-2)$ possess a unique steady state, whereas the single-magnon sectors support non-stationary dynamics with the Liouvillian restricted to them having purely imaginary eigenvalues [56, 66]. Since we are interested in the collective, synchronized dynamics of the local magnetization $\langle \sigma_\alpha^z(t) \rangle$, we focus on the single-magnon subspace $m = -N+2$, corresponding to a single spin-up excitation. All considerations equally apply to the corresponding spin-down sector $m = N-2$.

In Fig. 1 we show the time evolution of the local magnetization $\langle \sigma_\alpha^z(t) \rangle$ for three different motifs starting from random initial conditions within the single-magnon subspace: the \mathcal{C}_2 -symmetric motif in panel (a), the \mathcal{C}_4 -symmetric motif in panel (b), and the \mathcal{C}_6 -symmetric motif in panel (c). The insets depict the corresponding AB motif, with the central spin shown in blue, the inner spins in brown, and the dissipative outer spins in pink. Despite the different cyclic orders n , all motifs exhibit the same qualitative dynamics. The outer (pink) spins relax to a stationary magnetization on a timescale set by the dissipation rate γ , whereas the central (blue) spin and the

inner (brown) spins retain oscillations of finite amplitude. All inner spins evolve in full synchrony, while the central spin oscillates in anti-phase with them.

The observed dynamics arises from the interplay between quantum interference and dissipation. In the system without dissipation and in the presence of a gauge flux $\phi = \pi$, tunneling pathways interfere destructively through the AB effect, giving rise to localized wave packets (and flat bands in extended lattices), so-called AB cages [12]. In the AB motifs considered here, a local excitation of the central spin can coherently populate the inner spins, while destructive interference suppresses excitation of the outer spins. This behavior, however, occurs only when the initial state is fully localized at the central spin. For random initial conditions, multiple eigenmodes of the Hamiltonian with different frequencies contribute, resulting in unsynchronized dynamics, as illustrated by the gray lines in the background of Figs. 1a–c. When dissipation is introduced, any component of the dynamics not confined to the AB-caged subspace is damped out. The long-time dynamics is therefore restricted to this interference-protected subspace and exhibits oscillations reminiscent of AB caging in extended lattices. For this reason, we refer to these structures as AB motifs.

The dissipative dynamics of \mathcal{C}_n -symmetric motifs can be captured using concepts from quantum synchronization and the framework of strong dynamical symmetries; cf. Appendix A. The Liouvillian \mathcal{L} corresponding to Eqs. (1) and (2) possesses exactly one strong dynamical symmetry (see the Supplementary Material [65] for the proof), and therefore supports a single pair of purely imaginary eigenvalues $i\Omega_{\pm} = \pm i2\sqrt{n}g$ with corresponding Liouvillian eigenmodes $\varrho_+ = |\psi_+\rangle\langle\psi_-|$ and $\varrho_- = |\psi_-\rangle\langle\psi_+|$. The associated states are given by [65]

$$|\psi_{\pm}\rangle = \frac{1}{\sqrt{2}} \left(|c\rangle + \frac{1}{\sqrt{n}} \sum_{i=1}^n |i\rangle \right) \quad (3)$$

with $|j\rangle$ denoting the configuration with a single spin excitation at site $j \in \{c, 1, \dots, n\}$, and inherit the rotational \mathcal{C}_n symmetry of the motif. As a consequence of this strong dynamical symmetry, the long-time dynamics within the single-magnon subspace is dominated by the oscillatory contributions of ϱ_{\pm} . For generic initial conditions $\varrho(0)$ with nonzero overlap with this symmetry sector and after a transient time τ , the local spin magnetization of the central and inner spins for $t \geq \tau$ becomes (up to exponentially small corrections)

$$\langle\sigma_c^z(t)\rangle = A_c - 2|\langle\psi_+|\varrho(0)|\psi_-\rangle| \cos(\Omega t + \varphi), \quad (4)$$

$$\langle\sigma_i^z(t)\rangle = \bar{A} + \frac{2}{n}|\langle\psi_+|\varrho(0)|\psi_-\rangle| \cos(\Omega t + \varphi), \quad (5)$$

while the outer spins approach a constant value $\langle\sigma_{i,i+1}^z(t)\rangle = \bar{A}$. The constants A_c , \bar{A} and \bar{A} are determined by the initial condition and specified in the Supplementary Material [65]. The phase φ is defined

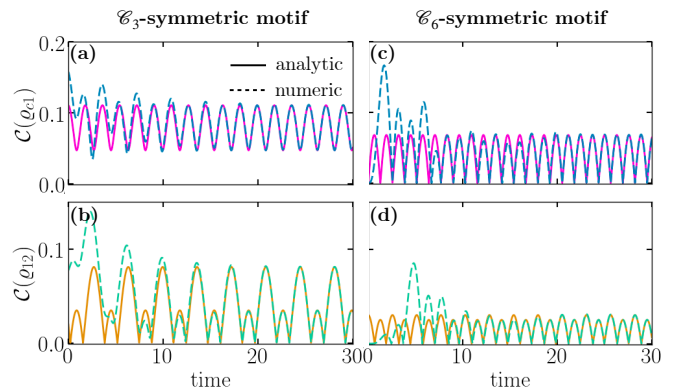


Figure 2. Concurrence as a measure of entanglement during the dissipative dynamics. Panels (a) and (b) show results for the \mathcal{C}_3 -symmetric motif with $N = 7$ spins, and panels (c) and (d) for the \mathcal{C}_6 -symmetric motif with $N = 13$ spins. The top panels display the concurrence between the central spin and an inner spin $\mathcal{C}(\varrho_{ci})$, which is identical for all inner spins due to rotational symmetry. The bottom panels show the concurrence between two inner spins $\mathcal{C}(\varrho_{ij})$, also identical for all inner-spin pairs. Solid lines correspond to the analytical expressions in Eqs. (6)–(7), including a numerically determined constant shift, while dashed lines show the full numerical results obtained from solving the Lindblad equation and include damped dynamics. The concurrence exhibits oscillations in time, reflecting the underlying synchronized spin dynamics. Parameters: $h = 1.0$, $g = 0.5$, $\phi = \pi$, $\gamma = 0.2$.

via $\langle\psi_+|\varrho(0)|\psi_-\rangle = |\langle\psi_+|\varrho(0)|\psi_-\rangle| \exp(i\varphi)$. Importantly, the same phase governs all oscillating spins, leading to synchronized motion within the motif as a direct consequence of quantum interference combined with spatially structured dissipation. This mechanism is considerably more robust than the purely coherent case: synchronization emerges for almost all initial states, except those orthogonal to the symmetry sector. The oscillation amplitude is maximal when the system is initialized with a single spin flip at the motif center, i.e. $\varrho(0) = |c\rangle\langle c|$.

Entanglement.—Interactions between spins in many-body systems naturally generate entanglement during their evolution. In open systems, however, dissipation and dephasing typically suppress such correlations [67]. Nevertheless, earlier studies have reported connections between synchronization and entanglement generation [48, 50–52], which motivates us to examine whether the synchronized spin dynamics in the AB motifs is accompanied by entanglement. To this end, we evaluate the concurrence, defined as $\mathcal{C}(\varrho_{\alpha\alpha'}) = \max\{0, \lambda_1 - \lambda_2 - \lambda_3 - \lambda_4\}$, where $\varrho_{\alpha\alpha'} = \text{Tr}_{\mathcal{A} \setminus \{\alpha, \alpha'\}}[\varrho(t)]$ is the reduced density matrix of spins α and α' , and \mathcal{A} denotes the collection of all indices α . The quantities λ_k are the square roots of the ordered eigenvalues of the matrix $\varrho_{\alpha\alpha'} \tilde{\varrho}_{\alpha\alpha'}$, with $\tilde{\varrho}_{\alpha\alpha'}$ denoting the spin-flipped state [68]. Owing to the rotational symmetry of the motifs, it is sufficient to consider only the concurrence between the central spin and any inner spin, $\mathcal{C}(\varrho_{ci})$, and that between two inner

spins, $\mathcal{C}(\varrho_{ij})$. Using this symmetry, we derive analytical expressions for the concurrence after the transient time, i.e., for $t \geq \tau$ [65],

$$\mathcal{C}(\varrho_{ci}) = 2C_c + \frac{1}{\sqrt{n}} \left| \tilde{C}_+ - 2i \langle \psi_+ | \varrho(0) | \psi_- \rangle \sin(\Omega t + \varphi) \right|, \quad (6)$$

$$\mathcal{C}(\varrho_{ij}) = 2\bar{C} + \frac{1}{n} \left| \tilde{C}_- + 2 \langle \psi_+ | \varrho(0) | \psi_- \rangle \cos(\Omega t + \varphi) \right|, \quad (7)$$

where C_c and \bar{C} denote contributions from components of the density matrix outside the strong-dynamical-symmetry subspace (which we obtain numerically below), and $\tilde{C}_\pm = \langle \psi_+ | \varrho(0) | \psi_+ \rangle \pm \langle \psi_- | \varrho(0) | \psi_- \rangle$. The oscillation frequency Ω and phase φ coincide with those in Eqs. (4) and (5). Note that for the system at hand, owing to the rotational symmetry, the concurrence is bounded by $0 \leq \mathcal{C}(\varrho_{ci}) \leq 1/\sqrt{n}$ and $0 \leq \mathcal{C}(\varrho_{ij}) \leq 1/n$ [65].

Figure 2 shows $\mathcal{C}(\varrho_{ci})$ [panels (a) and (c)] and $\mathcal{C}(\varrho_{ij})$ [panels (b) and (d)] for the \mathcal{C}_3 and \mathcal{C}_6 motifs. The solid lines are the analytical expressions from Eqs. (6)–(7), using numerically determined constants C_c and \bar{C} ; the dashed lines show the full numerical solutions of the Lindblad equation. After a short transient τ , the analytical and numerical results coincide. As the system size increases (larger n), the concurrence amplitude decreases, consistent with the reduced synchronization amplitude. The maximal concurrence within the strong-dynamical-symmetry subspace occurs for an initially localized excitation at the central spin, which mirrors the behavior of the synchronization amplitude [65].

Disorder.—Synchronization in the motifs relies on the exact cancellation of two tunneling paths at the outer spins, which may be difficult to realize perfectly in experiments. We therefore examine how disorder affects the synchronized spin dynamics. We first note that variations in the local dissipation rates $\gamma_{i,i+1}$ do not alter the long-time synchronized behavior as long as the dissipation channels remain strictly local. We thus focus on perturbations of the coherent dynamics by introducing disorder into H_n of Eq. (1), i.e., we consider $\tilde{H}_n = H_n + \varepsilon V$, where V can represent on-site or coupling disorder, including perturbations of the flux per plaquette.

Using non-Hermitian perturbation theory, one finds explicitly [65] that the first-order correction to the oscillatory Liouvillian eigenmodes with purely imaginary eigenvalues is again purely imaginary, producing only a frequency shift. A negative real correction can appear only at second order, leading to gradual damping of the synchronized dynamics and ultimately to a unique stationary state. However, for sufficiently weak perturbations, $\varepsilon^2 \ll g, \gamma$, the induced decay is slow: many oscillations occur before damping becomes appreciable, which renders the synchronized dynamics observable for long times. This regime corresponds to meta-stable synchronization [56].

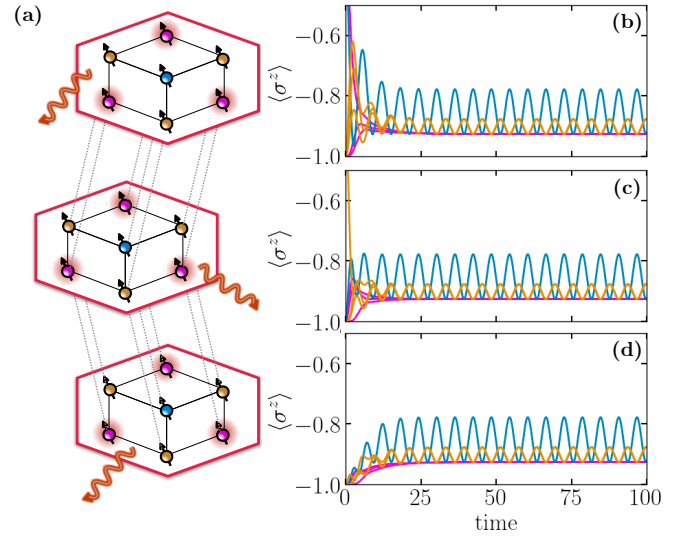


Figure 3. (a) Schematic representation of three coupled \mathcal{C}_3 -symmetric motifs. In addition to the intra-motif couplings, each spin in the middle motif is coupled to the corresponding spins in the top and bottom motifs (dashed lines). Collective dissipation, $L_\nu = \sqrt{\kappa} \sum_{\alpha \in \mathcal{A}} \sigma_{\alpha\nu}^z$ indicated by the red outline, acts on all spins within a motif labeled by ν . Panels (b)–(d) show the magnetization dynamics of the motifs shown on the left of each panel. After a short transient, the spins subject to strictly local dissipation (red discs) relax to stationary values (pink lines). The central (blue) spins become fully synchronized, both in amplitude and phase, across all three motifs. The inner (brown) spins also synchronize across motifs, with an oscillation amplitude equal to one third of that of the central spins, and evolve in anti-phase with them. Parameters: $h = 1.0$, $g = 0.3$, $\tilde{g} = 0.9g$, $\kappa = \gamma = 0.2$.

Synchronized Aharonov–Bohm Motifs.—We now couple the \mathcal{C}_n -symmetric motifs introduced above and include collective dissipation to synchronize the spin dynamics across motifs. Each motif, labeled by ν , is governed by its local Hamiltonian H_n^ν ; cf. Eq. (1). Inter-motif interactions are implemented via flip–flop couplings between corresponding spins in different motifs, described by

$$H_I^{\nu\nu'} = \tilde{g} \sum_{\alpha \in \mathcal{A}} (\sigma_{\alpha\nu}^+ \sigma_{\alpha\nu'}^- + \sigma_{\alpha\nu'}^+ \sigma_{\alpha\nu}^-), \quad (8)$$

where \tilde{g} is the inter-motif coupling strength and \mathcal{A} denotes all spin indices within a motif. Additionally, we include collective dissipation via $L_\nu = \sqrt{\kappa} \sum_{\alpha \in \mathcal{A}} \sigma_{\alpha\nu}^z$.

The interplay of collective intra-motif dissipation and coherent inter-motif coupling leads to complete synchronization of the spin dynamics across all motifs, as the components of the dynamics that are not synchronized are damped out. To illustrate this mechanism, we analyze three coupled \mathcal{C}_3 -symmetric motifs shown schematically in Fig. 3a. The red outlines indicate collective dissipation acting on all spins in each motif, while the dashed lines denote the inter-motif couplings. The result-

ing magnetization dynamics for each motif is displayed in Figs. 3b–d. After a transient time, the dynamics satisfies $\langle \sigma_{\alpha\nu}^z(t) \rangle = \langle \sigma_{\alpha\nu'}^z(t) \rangle$ for $t \geq \tau$ for all motifs ν, ν' . The oscillating spins (brown and blue) synchronize fully in both amplitude and phase with their respective spins across the motifs, following the same pattern as in the single-motif case [cf. Fig. 1], while the dissipative (pink) spins relax to identical stationary values across motifs. In contrast, without collective dissipation ($\kappa = 0$), synchronization is lost completely as shown Figs. 4 of Appendix B. Thus, it is the *combined* action of local dissipation, correlated dissipation, and a π -flux that enables global synchronization across motifs. This mechanism is not limited to the \mathcal{C}_3 geometry: any \mathcal{C}_n -symmetric AB motif can be coupled in this way, allowing synchronized dynamics to emerge across arbitrary networks of AB motifs.

Conclusions.—We have shown that the interplay of (synthetic) gauge fields and engineered dissipation can give rise to robust, synchronized spin dynamics in structures that we termed Aharonov–Bohm motifs. The local dissipation selectively damps components outside the interference-protected subspace, leaving behind oscillations that are stabilized by the motif’s rotational symmetry. We derived analytical expressions for the local magnetization and entanglement dynamics, confirmed by numerical simulations, and demonstrated how inter-motif coupling combined with correlated noise extends synchronization to larger networks.

These results establish a direct and previously unexplored connection between gauge fields, dissipation engineering, and quantum synchronization, which provides a robust mechanism for stabilizing collective many-body dynamics. The framework of dissipative Aharonov–Bohm motifs opens a route towards controlling nonequilibrium quantum phenomena in interference-driven flat-band systems, where the dynamics is dominated by strong correlations. An intriguing future direction is the inclusion of interactions (such as Ising-type couplings) which in closed systems are known to destroy Aharonov–Bohm caging [23]. In the dissipative setting, however, the interplay between interactions and engineered loss may instead stabilize new correlated phases or generate qualitatively different forms of synchronized many-body dynamics.

Acknowledgements.—The authors thank J. Liu and Q. Wu for helpful comments. G.P. acknowledges support from Spain’s MINECO through Grant No. PID2023-149072NBI00, CSIC Research Platform PTI-001, and National Project No. QTP2021-03-002. C.W.W. and G.P. received funding from the European Union’s Horizon Europe research and innovation programme under the Marie Skłodowska-Curie Actions (MSCA) grant agreement No. 101149948. Views and opinions expressed are, however, those of the author(s) only and do not necessarily reflect those of the European Union or the European Research Council. Neither the European Union nor

the granting authority can be held responsible for them.

* cwweachtler@icmm.csic.es

- [1] K. von Klitzing, The quantized Hall effect, *Rev. Mod. Phys.* **58**, 519 (1986).
- [2] D. C. Tsui, H. L. Stormer, and A. C. Gossard, Two-Dimensional Magnetotransport in the Extreme Quantum Limit, *Phys. Rev. Lett.* **48**, 1559 (1982).
- [3] D. Yoshioka, *The Quantum Hall Effect*, edited by M. Cardona, P. Fulde, K. Von Klitzing, H.-J. Queisser, R. Merlin, and H. Störmer, Springer Series in Solid-State Sciences, Vol. 133 (Springer, Berlin, Heidelberg, 2002).
- [4] Y.-J. Lin, R. L. Compton, K. Jiménez-García, J. V. Porto, and I. B. Spielman, Synthetic magnetic fields for ultracold neutral atoms, *Nature* **462**, 628 (2009).
- [5] M. Aidelsburger, M. Atala, M. Lohse, J. T. Barreiro, B. Paredes, and I. Bloch, Realization of the Hofstadter Hamiltonian with Ultracold Atoms in Optical Lattices, *Phys. Rev. Lett.* **111**, 185301 (2013).
- [6] M. Atala, M. Aidelsburger, M. Lohse, J. T. Barreiro, B. Paredes, and I. Bloch, Observation of chiral currents with ultracold atoms in bosonic ladders, *Nature Phys* **10**, 588 (2014).
- [7] F. A. An, E. J. Meier, and B. Gadway, Direct observation of chiral currents and magnetic reflection in atomic flux lattices, *Sci. Adv.* **3**, e1602685 (2017).
- [8] P. Roushan, C. Neill, A. Megrant, Y. Chen, R. Babbush, R. Barends, B. Campbell, Z. Chen, B. Chiaro, A. Dunsworth, A. Fowler, E. Jeffrey, J. Kelly, E. Lucero, J. Mutus, P. J. J. O’Malley, M. Neeley, C. Quintana, D. Sank, A. Vainsencher, J. Wenner, T. White, E. Kapit, H. Neven, and J. Martinis, Chiral ground-state currents of interacting photons in a synthetic magnetic field, *Nature Phys* **13**, 146 (2017).
- [9] C. Neill, T. McCourt, X. Mi, Z. Jiang, M. Y. Niu, W. Mruczkiewicz, I. Aleiner, F. Arute, K. Arya, J. Atalaya, R. Babbush, J. C. Bardin, R. Barends, A. Bengtsson, A. Bourassa, M. Broughton, B. B. Buckley, D. A. Buell, B. Burkett, N. Bushnell, J. Campero, Z. Chen, B. Chiaro, R. Collins, W. Courtney, S. Demura, A. R. Derk, A. Dunsworth, D. Eppens, C. Erickson, E. Farhi, A. G. Fowler, B. Foxen, C. Gidney, M. Giustina, J. A. Gross, M. P. Harrigan, S. D. Harrington, J. Hilton, A. Ho, S. Hong, T. Huang, W. J. Huggins, S. V. Isakov, M. Jacob-Mitos, E. Jeffrey, C. Jones, D. Kafri, K. Kechedzhi, J. Kelly, S. Kim, P. V. Klimov, A. N. Korotkov, F. Kostritsa, D. Landhuis, P. Laptev, E. Lucero, O. Martin, J. R. McClean, M. McEwen, A. Megrant, K. C. Miao, M. Mohseni, J. Mutus, O. Naaman, M. Neeley, M. Newman, T. E. O’Brien, A. Opremcak, E. Ostby, B. Pató, A. Petukhov, C. Quintana, N. Redd, N. C. Rubin, D. Sank, K. J. Satzinger, V. Shvarts, D. Strain, M. Szalay, M. D. Trevithick, B. Villalonga, T. C. White, Z. Yao, P. Yeh, A. Zalcman, H. Neven, S. Boixo, L. B. Ioffe, P. Roushan, Y. Chen, and V. Smelyanskiy, Accurately computing the electronic properties of a quantum ring, *Nature* **594**, 508 (2021).
- [10] Y. Shapira, T. Manovitz, N. Akerman, A. Stern, and R. Ozeri, Quantum Simulations of Interacting Systems with Broken Time-Reversal Symmetry, *Phys. Rev. X* **13**,

- 021021 (2023).
- [11] Y. Wang, Y.-K. Wu, Y. Jiang, M.-L. Cai, B.-W. Li, Q.-X. Mei, B.-X. Qi, Z.-C. Zhou, and L.-M. Duan, Realizing Synthetic Dimensions and Artificial Magnetic Flux in a Trapped-Ion Quantum Simulator, *Phys. Rev. Lett.* **132**, 130601 (2024).
- [12] J. Vidal, R. Mosseri, and B. Douçot, Aharonov-Bohm Cages in Two-Dimensional Structures, *Phys. Rev. Lett.* **81**, 5888 (1998).
- [13] J. Vidal, B. Douçot, R. Mosseri, and P. Butaud, Interaction Induced Delocalization for Two Particles in a Periodic Potential, *Phys. Rev. Lett.* **85**, 3906 (2000).
- [14] C. E. Creffield and G. Platero, Coherent Control of Interacting Particles Using Dynamical and Aharonov-Bohm Phases, *Phys. Rev. Lett.* **105**, 086804 (2010).
- [15] S. Mukherjee and R. R. Thomson, Observation of localized flat-band modes in a quasi-one-dimensional photonic rhombic lattice, *Opt. Lett.*, OL **40**, 5443 (2015).
- [16] M. Creutz, End States, Ladder Compounds, and Domain-Wall Fermions, *Phys. Rev. Lett.* **83**, 2636 (1999).
- [17] J. Zurita, C. E. Creffield, and G. Platero, Topology and Interactions in the Photonic Creutz and Creutz-Hubbard Ladders, *Advanced Quantum Technologies* **3**, 1900105 (2020).
- [18] C. C. Abilio, P. Butaud, Th. Fournier, B. Pannetier, J. Vidal, S. Tedesco, and B. Dalzotto, Magnetic Field Induced Localization in a Two-Dimensional Superconducting Wire Network, *Phys. Rev. Lett.* **83**, 5102 (1999).
- [19] C. Naud, G. Faini, and D. Mailly, Aharonov-Bohm Cages in 2D Normal Metal Networks, *Phys. Rev. Lett.* **86**, 5104 (2001).
- [20] S. Mukherjee, M. Di Liberto, P. Öhberg, R. R. Thomson, and N. Goldman, Experimental Observation of Aharonov-Bohm Cages in Photonic Lattices, *Phys. Rev. Lett.* **121**, 075502 (2018).
- [21] M. Kremer, I. Petrides, E. Meyer, M. Heinrich, O. Zilberberg, and A. Szameit, A square-root topological insulator with non-quantized indices realized with photonic Aharonov-Bohm cages, *Nat Commun* **11**, 907 (2020).
- [22] H. Li, Z. Dong, S. Longhi, Q. Liang, D. Xie, and B. Yan, Aharonov-Bohm Caging and Inverse Anderson Transition in Ultracold Atoms, *Phys. Rev. Lett.* **129**, 220403 (2022).
- [23] T. Chen, C. Huang, I. Velkovsky, T. Ozawa, H. Price, J. P. Covey, and B. Gadway, Interaction-driven breakdown of Aharonov-Bohm caging in flat-band Rydberg lattices, *Nat. Phys.* **21**, 221 (2025).
- [24] J. Zhang, W. Huang, J. Chu, J. Qiu, X. Sun, Z. Tao, J. Zhang, L. Zhang, Y. Zhou, Y. Chen, Y. Liu, S. Liu, Y. Zhong, J.-J. Miao, J. Niu, and D. Yu, Synthetic Multidimensional Aharonov-Bohm Cages in Fock State Lattices, *Phys. Rev. Lett.* **134**, 070601 (2025).
- [25] P. M. Harrington, E. J. Mueller, and K. W. Murch, Engineered dissipation for quantum information science, *Nat Rev Phys* **4**, 660 (2022).
- [26] F. Verstraete, M. M. Wolf, and J. Ignacio Cirac, Quantum computation and quantum-state engineering driven by dissipation, *Nature Phys* **5**, 633 (2009).
- [27] S. Diehl, E. Rico, M. A. Baranov, and P. Zoller, Topology by dissipation in atomic quantum wires, *Nature Phys* **7**, 971 (2011).
- [28] S. Diehl, A. Micheli, A. Kantian, B. Kraus, H. P. Büchler, and P. Zoller, Quantum states and phases in driven open quantum systems with cold atoms, *Nature Phys* **4**, 878 (2008).
- [29] F. Carollo, E. Gillman, H. Weimer, and I. Lesanovsky, Critical Behavior of the Quantum Contact Process in One Dimension, *Phys. Rev. Lett.* **123**, 100604 (2019).
- [30] M. Marcuzzi, M. Buchhold, S. Diehl, and I. Lesanovsky, Absorbing State Phase Transition with Competing Quantum and Classical Fluctuations, *Phys. Rev. Lett.* **116**, 245701 (2016).
- [31] E. Gillman, F. Carollo, and I. Lesanovsky, Nonequilibrium Phase Transitions in $(1+1)$ -Dimensional Quantum Cellular Automata with Controllable Quantum Correlations, *Phys. Rev. Lett.* **125**, 100403 (2020).
- [32] I. Lesanovsky, K. Macieszczak, and J. P. Garrahan, Nonequilibrium absorbing state phase transitions in discrete-time quantum cellular automaton dynamics on spin lattices, *Quantum Sci. Technol.* **4**, 02LT02 (2019).
- [33] E. Chertkov, Z. Cheng, A. C. Potter, S. Gopalakrishnan, T. M. Gatterman, J. A. Gerber, K. Gilmore, D. Gresh, A. Hall, A. Hankin, M. Matheny, T. Mengle, D. Hayes, B. Neyenhuis, R. Stutz, and M. Foss-Feig, Characterizing a non-equilibrium phase transition on a quantum computer, *Nat. Phys.* **19**, 1799 (2023).
- [34] T. E. Lee and H. R. Sadeghpour, Quantum synchronization of quantum van der Pol oscillators with trapped ions, *Phys. Rev. Lett.* **111**, 234101 (2013).
- [35] S. Walter, A. Nunnenkamp, and C. Bruder, Quantum synchronization of a driven self-sustained oscillator, *Phys. Rev. Lett.* **112**, 094102 (2014).
- [36] S. Walter, A. Nunnenkamp, and C. Bruder, Quantum synchronization of two van der Pol oscillators, *Ann. Phys.* **527**, 131 (2015).
- [37] S. Dutta and N. R. Cooper, Critical response of a quantum van der Pol oscillator, *Physical Review Letters* **123**, 250401 (2019).
- [38] N. Thomas and M. Senthilvelan, Quantum synchronization in quadratically coupled quantum van der Pol oscillators, *Phys. Rev. A* **106**, 012422 (2022).
- [39] N. Es' haqi-Sani, G. Manzano, R. Zambrini, and R. Fazio, Synchronization along quantum trajectories, *Phys. Rev. Research* **2**, 023101 (2020).
- [40] A. Delmonte, A. Romito, G. E. Santoro, and R. Fazio, Quantum effects on the synchronization dynamics of the Kuramoto model, *Phys. Rev. A* **108**, 032219 (2023).
- [41] Y. Shen, H. Y. Soh, W. Fan, and L.-C. Kwek, Enhancing quantum synchronization through homodyne measurement and squeezing, *arXiv preprint arXiv:2302.13465* (2023), [arXiv:2302.13465](https://arxiv.org/abs/2302.13465).
- [42] M. Xu, D. A. Tieri, E. C. Fine, J. K. Thompson, and M. J. Holland, Synchronization of Two Ensembles of Atoms, *Phys. Rev. Lett.* **113**, 154101 (2014).
- [43] C. W. Wächtler and G. Platero, Topological synchronization of quantum van der Pol oscillators, *Phys. Rev. Res.* **5**, 023021 (2023).
- [44] Y. J. Zhao, J. E. Moore, J. Thingna, and C. W. Wächtler, Quantum Synchronization of Perturbed Oscillating Coherences (2025), [arXiv:2510.11601](https://arxiv.org/abs/2510.11601) [quant-ph].
- [45] A. W. Laskar, P. Adhikary, S. Mondal, P. Katiyar, S. Vinjanampathy, and S. Ghosh, Observation of Quantum Phase Synchronization in Spin-1 Atoms, *Phys. Rev. Lett.* **125**, 013601 (2020).
- [46] M. Koppenhöfer, C. Bruder, and A. Roulet, Quantum synchronization on the IBM Q system, *Phys. Rev. Research* **2**, 023026 (2020).

- [47] Y. Li, Z. Xie, X. Yang, Y. Li, X. Zhao, X. Cheng, X. Peng, J. Li, E. Lutz, Y. Lin, and J. Du, *Experimental realization and synchronization of a quantum van der Pol oscillator* (2025), [arXiv:2504.00751](https://arxiv.org/abs/2504.00751) [quant-ph].
- [48] Z. Tao, F. Schmolke, C.-K. Hu, W. Huang, Y. Zhou, J. Zhang, J. Chu, L. Zhang, X. Sun, Z. Guo, J. Niu, W. Weng, S. Liu, Y. Zhong, D. Tan, D. Yu, and E. Lutz, Noise-induced quantum synchronization with entangled oscillations, *Nat Commun* **16**, 8457 (2025).
- [49] J. Liu, Q. Wu, J. E. Moore, H. Haeffner, and C. W. Wächtler, Observation of synchronization between two quantum van der Pol oscillators in trapped ions (2025), [arXiv:2509.18423](https://arxiv.org/abs/2509.18423) [quant-ph].
- [50] T. E. Lee, C.-K. Chan, and S. Wang, Entanglement tongue and quantum synchronization of disordered oscillators, *Phys. Rev. E* **89**, 022913 (2014).
- [51] A. Roulet and C. Bruder, Quantum synchronization and entanglement generation, *Phys. Rev. Lett.* **121**, 063601 (2018).
- [52] F. Schmolke and E. Lutz, Noise-induced quantum synchronization, *Physical Review Letters* **129**, 250601 (2022).
- [53] G. L. Giorgi, F. Galve, G. Manzano, P. Colet, and R. Zambrini, Quantum correlations and mutual synchronization, *Phys. Rev. A* **85**, 052101 (2012).
- [54] N. Lörch, S. E. Nigg, A. Nunnenkamp, R. P. Tiwari, and C. Bruder, Quantum synchronization blockade: Energy quantization hinders synchronization of identical oscillators, *Phys. Rev. Lett.* **118**, 243602 (2017).
- [55] T. Kehrer, T. Nadolny, and C. Bruder, Quantum synchronization through the interference blockade, *Phys. Rev. A* **110**, 042203 (2024).
- [56] B. Buča, C. Booker, and D. Jaksch, Algebraic theory of quantum synchronization and limit cycles under dissipation, *SciPost Phys.* **12**, 097 (2022).
- [57] J. Tindall, C. Sánchez Muñoz, B. Buča, and D. Jaksch, Quantum synchronisation enabled by dynamical symmetries and dissipation, *New J. Phys.* **22**, 013026 (2020).
- [58] C. W. Wächtler and J. E. Moore, Topological quantum synchronization of fractionalized spins, *Phys. Rev. Lett.* **132**, 196601 (2024).
- [59] J. Zurita, C. Creffield, and G. Platero, Tunable zero modes and quantum interferences in flat-band topological insulators, *Quantum* **5**, 591 (2021).
- [60] J. Zurita, C. E. Creffield, and G. Platero, Hidden topology in flat-band topological insulators: Strong, weak, and square-root topological states, *Phys. Rev. B* **111**, 155406 (2025).
- [61] W. Feng, D. Shao, G.-Q. Zhang, Q.-P. Su, J.-X. Zhang, and C.-P. Yang, Quantum simulation of Hofstadter butterfly with synthetic gauge fields on two-dimensional superconducting-qubit lattices, *Front. Phys.* **18**, 61302 (2023).
- [62] X. Li, Y. Ma, J. Han, T. Chen, Y. Xu, W. Cai, H. Wang, Y. Song, Z.-Y. Xue, Z.-q. Yin, and L. Sun, Perfect Quantum State Transfer in a Superconducting Qubit Chain with Parametrically Tunable Couplings, *Phys. Rev. Applied* **10**, 054009 (2018).
- [63] T. Manovitz, Y. Shapira, N. Akerman, A. Stern, and R. Ozeri, Quantum Simulations with Complex Geometries and Synthetic Gauge Fields in a Trapped Ion Chain, *PRX Quantum* **1**, 020303 (2020).
- [64] M. Cattaneo, M. A. Rossi, G. García-Pérez, R. Zambrini, and S. Maniscalco, Quantum Simulation of Dissipative Collective Effects on Noisy Quantum Computers, *PRX Quantum* **4**, 010324 (2023).
- [65] See Supplemental Material [url] for (I) the spectral decomposition of the Liouvillian superoperator, (II) the proof of the synchronization condition, (III) the analytic expression of the local spin magnetization, and (IV) the Liouvillian perturbation theory; includes Ref. [69].
- [66] B. Buča, J. Tindall, and D. Jaksch, Non-stationary coherent quantum many-body dynamics through dissipation, *Nature Communications* **10**, 1730 (2019).
- [67] J. Dias, C. W. Wächtler, K. Nemoto, and W. J. Munro, Entanglement generation between distant spins via quasilocal reservoir engineering, *Phys. Rev. Res.* **5**, 043295 (2023).
- [68] W. K. Wootters, Entanglement of Formation of an Arbitrary State of Two Qubits, *Phys. Rev. Lett.* **80**, 2245 (1998).
- [69] M.-J. Zhao, T. Ma, Z. Wang, S.-M. Fei, and R. Pereira, Coherence concurrence for X states, *Quantum Inf Process* **19**, 104 (2020).

END MATTER

Appendix A: Strong dynamical symmetries and synchronization of local observables.—Quantum synchronization, as discussed in the main text, refers to the emergence of persistent, synchronized oscillations of local observables in the long-time limit. Such oscillations are associated with purely imaginary eigenvalues of the Liouvillian \mathcal{L} . A robust route to guarantee the existence of these eigenmodes is through the presence of a strong dynamical symmetry [56, 57, 66]. Consider a generic Lindblad master equation

$$\dot{\rho} = -i[H, \rho] + \sum_{\mu} \left(L_{\mu} \rho L_{\mu}^{\dagger} - \frac{1}{2} \{L_{\mu}^{\dagger} L_{\mu}, \rho\} \right) \equiv \mathcal{L}[\rho], \quad (9)$$

with system Hamiltonian H and Lindblad operators L_{μ} . If there exists an operator A that is an eigenoperator of the Hamiltonian, $[H, A] = \lambda A$, and simultaneously commutes with all Lindblad operators, $[L_{\mu}, A] = 0 = [L_{\mu}^{\dagger}, A]$, then the Liouvillian possesses at least one pair of purely imaginary eigenvalues $\pm i\lambda$,

$$\mathcal{L}[\rho_{\pm}] = \pm i\lambda \rho_{\pm}. \quad (10)$$

While a strong dynamical symmetry guarantees persistent oscillations in the steady-state manifold, synchronization of *local* observables requires an additional permutation symmetry among subsystems. Let P_{jk} denote the operator that exchanges subsystems j and k (e.g. spins in the AB motifs of the main text), and define the corresponding superoperator $\mathcal{P}_{jk}[x] = P_{jk} x P_{jk}$. If \mathcal{P}_{jk} is a weak symmetry of the Liouvillian, $[\mathcal{L}, \mathcal{P}_{jk}] = 0$, and commutes with the operator A , i.e. $P_{jk} A P_{jk} = A$, then the dynamics of the two local observables O_j and O_k are synchronized whenever $\text{Tr}[O_j \rho_{\pm}] \neq 0$. That is, after a

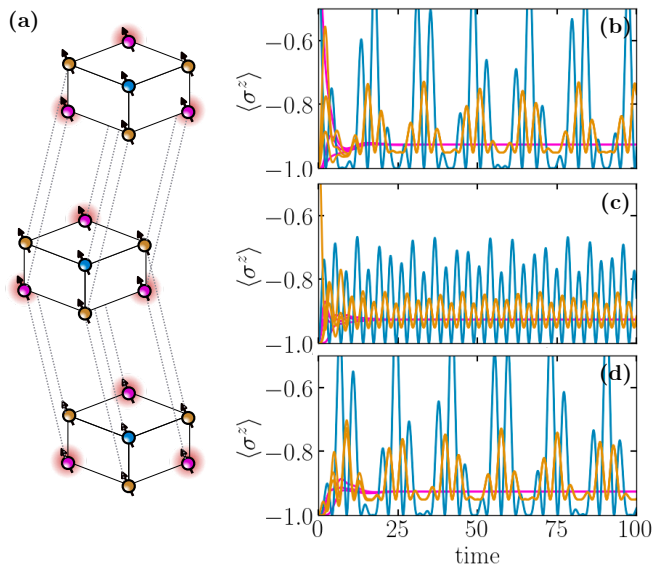


Figure 4. (a) Schematic representation of three coupled \mathcal{C}_3 -symmetric motifs, which do not synchronize in the absence of collective dissipation (compared to Fig. 3a in the main text). Panels (b)–(d) show the corresponding local magnetization dynamics for the motifs depicted to the left of each panel, now without the collective intra-motif dissipation. Although local dissipation is present, the long-term dynamics exhibits no synchronization, neither across motifs nor within each motif individually. Colors match those used in Fig. 3(b–d) and the spin coloring in panel (a). Parameters: $h = 1.0$, $g = 0.3$, $\tilde{g} = 0.9g$, $\kappa = 2\gamma = 0.4$.

transient time τ ,

$$\langle O_j(t) \rangle = \langle O_k(t) \rangle \quad \forall t \geq \tau, \quad (11)$$

up to exponentially small corrections.

Appendix B: Loss of inter-motif synchronization.—The emergence of fully synchronized spin dynamics across coupled AB motifs relies critically on the presence of additional collective intra-motif dissipation. To illustrate this explicitly, Figs. 4b–d show the local magnetization dynamics in the absence of collective dissipation (while retaining the same local loss processes), using identical parameters and initial conditions as in Fig. 3. Each panel (b)–(d) displays the dynamics of the motif depicted to its left [panel (a)]. As discussed in the main text, when the collective channel is removed the synchronized oscillations disappear: not only is phase locking between motifs lost, but the inter-motif coupling also disrupts the residual intra-motif synchronization.

Supplementary Material to 'Synchronized Aharonov-Bohm Motifs via Engineered Dissipation'

I. SPECTRAL DECOMPOSITION OF THE LIOUVILLIAN SUPEROPERATOR

Throughout this Supplementary Material, we frequently use a superoperator notation, which we summarize here for convenience. Consider a general Lindblad master equation of the form $\dot{\varrho} = \mathcal{L}[\varrho]$ where the Liouvillian superoperator \mathcal{L} acts as

$$\mathcal{L}[\varrho] = -i[H, \varrho] + \sum_{\mu} \left(L_{\mu} \varrho L_{\mu}^{\dagger} - \frac{1}{2} \{L_{\mu}^{\dagger} L_{\mu}, \varrho\} \right). \quad (\text{S1})$$

The Liouvillian can be written in its spectral decomposition,

$$\mathcal{L} = \sum_k \lambda_k |\varrho_k\rangle\rangle \langle\langle \sigma_k|, \quad (\text{S2})$$

where $\lambda_k \in \mathbb{C}$ are the complex eigenvalues and $|\varrho_k\rangle\rangle$ and $\langle\langle \sigma_k|$ denote the right and left eigenstates of \mathcal{L} , respectively. These satisfy

$$\mathcal{L} |\varrho_k\rangle\rangle = \lambda_k |\varrho_k\rangle\rangle, \quad \mathcal{L}^{\dagger} |\sigma_k\rangle\rangle = \lambda_k^* |\sigma_k\rangle\rangle, \quad \langle\langle \sigma_k | \varrho_{k'} \rangle\rangle = \delta_{k,k'}, \quad (\text{S3})$$

with $\langle\langle \sigma | \varrho \rangle\rangle = \text{Tr}(\sigma^{\dagger} \varrho)$ the Hilbert-Schmidt inner product. The formal solution of the master equation for an initial state $\varrho(0)$ is then

$$|\varrho(t)\rangle\rangle = \sum_k \exp(\lambda_k t) |\varrho_k\rangle\rangle \langle\langle \sigma_k | \varrho(0) \rangle\rangle. \quad (\text{S4})$$

Consequently, the expectation value of an observable O evolves as

$$\langle O(t) \rangle = \text{Tr}[O \varrho(t)] = \sum_k \exp(\lambda_k t) \langle\langle O | \varrho_k \rangle\rangle \langle\langle \sigma_k | \varrho(0) \rangle\rangle. \quad (\text{S5})$$

II. SYNCHRONIZATION CONDITION FOR \mathcal{C}_n -SYMMETRIC AHARONOV-BOHM MOTIFS

For the dissipative Aharonov-Bohm (AB) motifs with \mathcal{C}_n rotational symmetry discussed in the main text to exhibit stable synchronization—meaning that generic initial states lead to synchronized dynamics of the local magnetization $\langle \sigma_i^z(t) \rangle$ after a transient time—the following two key properties must hold, and we prove them in this section:

- (i) In the single-magnon subspaces with total magnetization $m = \pm(N - 2)$, there exists exactly one strong dynamical symmetry (see also Appendix A). This symmetry gives rise to the oscillatory Liouvillian eigenmodes responsible for synchronized dynamics of the local observables $\langle \sigma_i^z(t) \rangle$.
- (ii) All remaining magnetization sectors with $m \neq \pm(N + 2)$ contain at most a single steady state and do not support oscillations; they contribute only a static offset and therefore do not affect synchronization.

We first analyze these conditions for a single four-spin plaquette and then generalize our arguments to arbitrary \mathcal{C}_n -symmetric motifs.

Synchronization condition of a single spin plaquette with $N = 4$

We begin with a single plaquette of $N = 4$ spins described by the Hamiltonian (note that the labels used here differ slightly from those in the main text for the AB motifs)

$$H_{\text{plaq}} = h \sum_{i=1}^4 \sigma_i^z + g \sum_{i=1}^4 (e^{i\phi_i} \sigma_{i+1}^+ \sigma_i^- + \text{h.c.}), \quad (\text{S6})$$

where the total flux through the plaquette is $\phi = \sum_{\square} \phi_i$, and periodic boundary conditions $5 \equiv 1$ are imposed. Local dissipation acts on spin $i = 3$ via the Lindblad operator $L = \sqrt{\gamma}\sigma_3^z$; cf. Eq. (2).

Because the plaquette is equivalent to a one-dimensional chain, the dynamics can be solved by mapping spin operators to spinless fermions through the Jordan–Wigner transformation. The transformed Hamiltonian becomes

$$\tilde{H}_{\text{plaq}} = h \sum_{i=1}^4 (2n_i - 1) + g \sum_{i=1}^3 \left(e^{i\phi_i} c_{i+1}^\dagger c_i + \text{h.c.} \right) + g(-1)^{(\bar{n}-1)} \left(e^{i\phi_4} c_1^\dagger c_4 + \text{h.c.} \right), \quad (\text{S7})$$

where $\bar{n} = \sum_j n_j = \sum_j c_j^\dagger c_j$ is the total fermion number. The fermionic and spin operators satisfy

$$\sigma_j^+ = \exp\left(-i\pi \sum_{l=1}^{j-1} n_l\right) c_j^\dagger, \quad \sigma_j^- = \exp\left(i\pi \sum_{l=1}^{j-1} n_l\right) c_j. \quad (\text{S8})$$

We first consider the single-excitation subspace (or single-magnon subspace in spin language). Synchronization of local observables requires the existence of exactly one strong dynamical symmetry in the single-magnon sector, i.e., there exists an operator A which is an eigenoperator of the Hamiltonian and that commutes with the dissipator $L = \sqrt{\gamma}(2n_3 - 1)$. For flux $\phi = \pi$, the Hamiltonian H_{plaq} possesses eigenvalues $E_{\pm} = h \pm \sqrt{2}g$, each twofold degenerate. A convenient choice of normalized eigenvectors spanning the degenerate subspaces is

$$|v_-^{(1)}\rangle = \frac{1}{2} \begin{pmatrix} \sqrt{2} \\ -1 \\ 0 \\ 1 \end{pmatrix}, \quad |v_-^{(2)}\rangle = \frac{1}{2} \begin{pmatrix} 1 \\ -\sqrt{2} \\ 1 \\ 0 \end{pmatrix}, \quad |v_+^{(1)}\rangle = \frac{1}{2} \begin{pmatrix} -\sqrt{2} \\ -1 \\ 0 \\ 1 \end{pmatrix}, \quad |v_+^{(2)}\rangle = \frac{1}{2} \begin{pmatrix} 1 \\ \sqrt{2} \\ 1 \\ 0 \end{pmatrix}. \quad (\text{S9})$$

The operator $A = |v_-^{(1)}\rangle \langle v_+^{(1)}|$ fulfills the conditions for a strong dynamical symmetry (cf. Appendix A), because both states, $|v_-^{(1)}\rangle$ and $|v_+^{(1)}\rangle$, have zero amplitude on dissipative site $i = 3$, and therefore are eigenstates of $(2n_3 - 1)$ (or equivalently σ_3^z in the original spin picture) with eigenvalue -1 , while being eigenstates of the Hamiltonian with energies E_{\pm} . The other eigenstates are not eigenvectors of σ_3^z and thus do not satisfy the dynamical symmetry condition.

Within the resulting two-dimensional strong-dynamical symmetry subspace, the density matrix evolves as

$$\varrho(t) = \langle v_-^{(1)} | \varrho(0) | v_-^{(1)} \rangle \varrho_- + \langle v_+^{(1)} | \varrho(0) | v_+^{(1)} \rangle \varrho_+ + \left[e^{-i\Omega t} \langle v_+^{(1)} | \varrho(0) | v_-^{(1)} \rangle + \text{h.c.} \right], \quad (\text{S10})$$

where $\varrho_- = |v_-^{(1)}\rangle \langle v_-^{(1)}|$, $\varrho_+ = |v_+^{(1)}\rangle \langle v_+^{(1)}|$, and the oscillation frequency is $\Omega = E_+ - E_- = 2\sqrt{2}g$. The local observables exhibit then synchronized oscillations; explicitly,

$$\langle \sigma_1^z(t) \rangle \propto -2 \left| \langle v_+^{(1)} | \varrho(0) | v_-^{(1)} \rangle \right| \cos(2\sqrt{2}gt) \quad \langle \sigma_2^z(t) \rangle = \langle \sigma_4^z(t) \rangle \propto \left| \langle v_+^{(2)} | \varrho(0) | v_-^{(2)} \rangle \right| \cos(2\sqrt{2}gt), \quad (\text{S11})$$

demonstrating perfect synchronization among the non-dissipative spins.

Because both the Hamiltonian and dissipator are quadratic in the fermionic operators, every two-particle state is constructed from single-particle orbitals. For the double-excitation subspace to support nontrivial oscillatory dynamics, a two-dimensional dark subspace would be required; i.e., both fermions must occupy orbitals with zero amplitude on site $i = 3$, ensuring $n_3 = 0$ and thus an eigenvalue of -1 of $(2n_3 - 1)$. However, from the structure of the single-particle eigenstates, only one such two-particle state exists. Therefore the two-excitation sector contains only a *one-dimensional* dark space and no strong dynamical symmetry. Consequently, it supports no oscillatory dynamics. The three-excitation (single-hole) subspace is equivalent to the single-excitation sector by particle–hole symmetry and therefore exhibits the same structure: one strong dynamical symmetry and the same oscillation frequency.

Smallest motif with \mathcal{C}_2 -rotational symmetry

After establishing that the plaquette hosts a single strong dynamical symmetry in the one-magnon manifold, we now show that an analogous structure appears in the smallest AB motif with rotational symmetry. In contrast to the plaquette, no simple mapping to free fermions exists. Nevertheless, the \mathcal{C}_2 symmetry allows one to identify a two-dimensional strong-dynamical symmetry subspace in the single-magnon sector, while all remaining magnetization sectors contain at most one dark state.

The \mathcal{C}_2 -symmetric motif consists of five spins; see the inset of Fig. 3a. As before, we seek eigenstates with zero weight on the two outer spins where dissipation acts. Because of the rotation symmetry, this condition must hold for both outer spins simultaneously, since $C_2\sigma_3^z C_2^{-1} = \sigma_5^z$ and vice versa.

The Hamiltonian is given by H_n of the main text with $n = 2$ [see Eq. (1)], and the dissipative dynamics by the Lindblad equation in Eq. (2). Projecting into the one-magnon subspace using $\mathcal{P}_n = \sum_{\alpha \in \mathcal{A}_n} |\alpha\rangle \langle \alpha|$, with $|\alpha\rangle$ denoting a configuration with a single spin-up excitation, we obtain the projected Hamiltonian for the \mathcal{C}_2 -symmetric motif $\tilde{H}_2 = \mathcal{P}H_2\mathcal{P}$. With the gauged fixed such that the flux per plaquette is $\phi = \pi$ and at the outer boundaries of the plaquettes,

$$\tilde{H}_2 = h \sum_{\alpha} |\alpha\rangle \langle \alpha| + g(|c\rangle \langle 1| + i|(1,2)\rangle \langle 1| + i|2\rangle \langle (1,2)| + |c\rangle \langle 2| + i|(2,1)\rangle \langle 2| + i|1\rangle \langle (2,1)| + \text{h.c.}). \quad (\text{S12})$$

A state with no excitation on the outer sites $\alpha = (1,2)$ or $\alpha = (2,1)$ takes the form $|\psi\rangle = a_c |c\rangle + a_1 |1\rangle + a_2 |2\rangle$. Since, $[H_2, C_2] = 0$, eigenstates of H_2 can be chosen to satisfy $C_2 |\psi\rangle = \pm |\psi\rangle$. This yields the symmetry-adapted combinations

$$|\psi_{\pm}\rangle = a_c |c\rangle + a_1 (|1\rangle \pm |2\rangle). \quad (\text{S13})$$

The antisymmetric combination $|\psi_{-}\rangle$ is not an eigenstate of \tilde{H}_2 , while the symmetric state $|\psi_{+}\rangle$ satisfies

$$\tilde{H}_2 |\psi_{+}\rangle = h |\psi_{+}\rangle + a_c g(|1\rangle + |2\rangle) + 2ga_1 |1\rangle = E |\psi_{+}\rangle. \quad (\text{S14})$$

This yields $a_c = \pm\sqrt{2}a_1$, corresponding to two eigenstates with energies $E_{\pm} = h \pm \sqrt{2}g$. Fixing normalization sets $a_1 = 1/2$. Thus, the single-magnon subspace contains a two-dimensional strong-dynamical symmetry subspace spanned by two eigenstates with distinct energies. Consequently, the resulting dynamics of the density matrix is analogous to Eq. (S10).

We now examine the two-excitation manifold. A dark state must be an eigenstate of both dissipators $\sigma_{1,2}^z$, $\sigma_{2,1}^z$, and the rotation operator C_2 . Let $|\psi\rangle$ satisfy

$$\sigma_{1,2}^z |\psi\rangle = z_{1,2} |\psi\rangle, \quad \sigma_{2,1}^z |\psi\rangle = z_{2,1} |\psi\rangle, \quad C_2 |\psi\rangle = p |\psi\rangle, \quad (\text{S15})$$

where $z_{1,2}, z_{2,1}, p \in \{\pm 1\}$. Using $C_2\sigma_{1,2}^z = \sigma_{2,1}^z C_2$ gives

$$z_{1,2} p |\psi\rangle = \sigma_{1,2}^z C_2 |\psi\rangle = C_2 \sigma_{2,1}^z |\psi\rangle = z_{2,1} p |\psi\rangle, \quad (\text{S16})$$

which implies $z_{1,2} = z_{2,1}$. If both equal $+1$, the excitations occupy only the outer spins; this configuration is not an eigenstate of the Hamiltonian because hopping is allowed on the connected graph. The only remaining case is $z_{1,2} = z_{2,1} = -1$, implying that the state has no support on the outer spins.

Restricting to the corresponding inner-excitation subspace, $\mathcal{P}_{\text{inner}} = \text{span}\{|c1\rangle, |c2\rangle, |12\rangle\}$, the action of C_2 gives $C_2 |c1\rangle = |c2\rangle$ and $C_2 |12\rangle = |12\rangle$. Thus, the subspace decomposes into symmetric and antisymmetric sectors according to the eigenvalue of C_2 :

$$\mathcal{P}_{\text{inner}}^{(+)} = \text{span}\left\{|12\rangle, \frac{1}{\sqrt{2}}(|c1\rangle + |c2\rangle)\right\}, \quad \mathcal{P}_{\text{inner}}^{(-)} = \text{span}\left\{\frac{1}{\sqrt{2}}(|c1\rangle - |c2\rangle)\right\}. \quad (\text{S17})$$

We now examine whether these subspaces are invariant under the Hamiltonian \tilde{H}_2 . Acting with \tilde{H}_2 on states of $\mathcal{P}_{\text{inner}}^{(+)}$ shows that they are not preserved within $\mathcal{P}_{\text{inner}}^{(+)}$, that is, they ‘leak’ into states involving the outer spins. In contrast, the antisymmetric subspace $\mathcal{P}_{\text{inner}}^{(-)}$ remains invariant under \tilde{H}_2 . However, as $\mathcal{P}_{\text{inner}}^{(-)}$ is one-dimensional, it contains only a single such state and therefore does not support a two-dimensional subspace capable of sustaining oscillatory dynamics. Thus, the two-magnon manifold contributes only static, non-oscillatory corrections to long-time local observables.

General motif with \mathcal{C}_n -symmetry

We now extend the previous analysis to a motif composed of n plaquettes with \mathcal{C}_n -rotational symmetry. Using the same symmetry constraints as before, we show that synchronized oscillations arise exclusively within the one-magnon manifold, while all other magnon sectors contribute only static long-time dynamics.

Dark states must be simultaneous eigenstates of the rotation operator C_n and of all $\sigma_{i,i+1}^z$. Since $C_n \sigma_{i,i+1}^z C_n^{-1} = \sigma_{i+1,i+2}^z$, the eigenvalue conditions enforce $z_{i,i+1} = -1$ for all i , implying that a dark state must have zero weight on all outer spins. Solving these constraints yields precisely two one-magnon states,

$$|\psi_{\pm}\rangle = \frac{1}{\sqrt{2}} \left(\pm |c\rangle + \frac{1}{\sqrt{n}} \sum_{i=1}^n |i\rangle \right), \quad (\text{S18})$$

with energies $E_{\pm} = h \pm \sqrt{n}g$. Thus, each single-magnon sector contains a two-dimensional strong-dynamical symmetry subspace spanned by $|\psi_{\pm}\rangle$.

For two excitations, the ‘no-leakage’ condition (vanishing amplitude on all outer spins) translates to

$$\sigma_{i,i+1}^+ (\sigma_i^- - \sigma_{i+1}^-) |\psi\rangle = 0 \quad \forall i. \quad (\text{S19})$$

Exploiting \mathcal{C}_n symmetry, a convenient basis for the inner two-excitation subspace is

$$|C_l\rangle = \frac{1}{\sqrt{n}} \sum_i \lambda^{li} |ci\rangle, \quad |I_l\rangle = \frac{1}{\sqrt{x}} \sum_i \lambda^{li} |ii+1\rangle, \quad \lambda = e^{2\pi i/n}. \quad (\text{S20})$$

Evaluating the constraint shows that only the totally symmetric state $|C_0\rangle$ satisfies the no-leakage condition; all other states necessarily hybridize with outer-spin configurations and are therefore not dark. Hence, the two-magnon manifold contains a single dark state.

The same argument extends to all higher-excitation sectors: only the one-magnon spaces possess a two-dimensional invariant subspace capable of supporting coherent oscillations. All higher-magnon sectors contribute solely static, non-oscillatory corrections to the long-time behavior of local observables.

III. ANALYTIC EXPRESSION OF THE LOCAL SPIN MAGNETIZATION DYNAMICS

As established above, only the single-magnon manifolds contribute to oscillatory dynamics; all higher-excitation sectors yield static long-time behavior. We therefore restrict the analysis to the one-magnon subspace. Each such subspace hosts a single strong dynamical symmetry and an associated two-dimensional manifold spanned by the eigenstates $|\psi_{\pm}\rangle$; cf. Eq. (S18). In all examples considered in the main text, we find precisely one additional stationary mode $|\bar{\varrho}\rangle$ not connected to the dynamical-symmetry sector, satisfying $\mathcal{L}[\bar{\varrho}] = 0$. For clarity, we include only this mode; additional stationary contributions from other excitation sectors can be evaluated analogously.

Using the spectral decomposition of the Liouvillian, Eq. (S2), the long-time limit of the density matrix from Eq. (S4) becomes

$$\lim_{t \rightarrow \infty} |\varrho(t)\rangle\rangle = |\bar{\varrho}\rangle\rangle \langle\langle \bar{\sigma} | + |\varrho_{++}\rangle\rangle \langle\langle \sigma_{++} | + |\varrho_{--}\rangle\rangle \langle\langle \sigma_{--} | + e^{i\Omega t} |\varrho_{+-}\rangle\rangle \langle\langle \sigma_{+-} | + e^{-i\Omega t} |\varrho_{-+}\rangle\rangle \langle\langle \sigma_{-+} |, \quad (\text{S21})$$

where $|\varrho_{\nu\nu'}\rangle\rangle$ denotes the vectorized operator $|\psi_{\nu}\rangle\langle\psi_{\nu'}|$ with $|\psi_{\nu}\rangle$ given by Eq. (S18) for $\nu = \pm$.

The expectation value of any operator σ_{α}^z follows as

$$\lim_{t \rightarrow \infty} \langle\sigma_{\alpha}^z(t)\rangle = \langle\langle \sigma_{\alpha}^z | \bar{\varrho} \rangle\rangle \langle\langle \bar{\sigma} | \varrho(0) \rangle\rangle + \sum_{\nu=\pm} \langle\langle \sigma_{\alpha}^z | \varrho_{\nu\nu} \rangle\rangle \langle\langle \sigma_{\nu\nu} | \varrho(0) \rangle\rangle + e^{i\Omega t} \langle\langle \sigma_{\alpha}^z | \varrho_{+-} \rangle\rangle \langle\langle \sigma_{+-} | \varrho(0) \rangle\rangle + e^{-i\Omega t} \langle\langle \sigma_{\alpha}^z | \varrho_{-+} \rangle\rangle \langle\langle \sigma_{-+} | \varrho(0) \rangle\rangle. \quad (\text{S22})$$

Note, that $\langle\langle \sigma_{\nu\nu'} | \varrho(0) \rangle\rangle = \langle\psi_{\nu} | \varrho(0) | \psi_{\nu'}\rangle$ and similarly $\langle\langle \sigma_{\alpha}^z | \varrho_{\nu\nu'} \rangle\rangle = \langle\psi_{\nu'} | \sigma_{\alpha}^z | \psi_{\nu}\rangle$. Evaluating the different terms of Eq. (S22) by plugging in Eq. (3), one then finds the expressions of the main text for the local spin magnetization, namely

$$\langle\sigma_c^z(t)\rangle = A_c - 2 |\langle\psi_+ | \varrho(0) | \psi_-\rangle| \cos(\Omega t + \varphi), \quad \langle\sigma_i^z(t)\rangle = \bar{A} + \frac{2}{n} |\langle\psi_+ | \varrho(0) | \psi_-\rangle| \cos(\Omega t + \varphi), \quad \langle\sigma_{i,i+1}^z(t)\rangle = \tilde{A}. \quad (\text{S23})$$

The constants are given by

$$A_c = \langle\langle \sigma_c^z | \bar{\varrho} \rangle\rangle \langle\langle \bar{\sigma} | \varrho(0) \rangle\rangle, \quad (\text{S24})$$

$$\bar{A} = \langle\langle \sigma_i^z | \bar{\varrho} \rangle\rangle \langle\langle \bar{\sigma} | \varrho(0) \rangle\rangle + \left(\frac{1}{n} - 1 \right) (\langle\psi_+ | \varrho(0) | \varrho_+\rangle + \langle\psi_- | \varrho(0) | \varrho_-\rangle), \quad (\text{S25})$$

$$\tilde{A} = \langle\langle \sigma_{i,i+1}^z | \bar{\varrho} \rangle\rangle \langle\langle \bar{\sigma} | \varrho(0) \rangle\rangle - (\langle\psi_+ | \varrho(0) | \varrho_+\rangle + \langle\psi_- | \varrho(0) | \varrho_-\rangle) \quad (\text{S26})$$

Note that $\langle\psi_{\nu} | \sigma_c^z | \psi_{\nu}\rangle = 0$ and $\langle\psi_{\nu} | \sigma_i^z | \psi_{\nu}\rangle = -1 + 1/n$.

IV. ANALYTIC EXPRESSION OF CONCURRENCE BETWEEN TWO SPINS

To characterize the entanglement generated by synchronized dynamics in a \mathcal{C}_n -symmetric motif, we evaluate the concurrence \mathcal{C} , defined by

$$\mathcal{C}(\varrho_{\alpha\alpha'}) = \max\{0, \lambda_1 - \lambda_2 - \lambda_3 - \lambda_4\}, \quad (\text{S27})$$

where $\varrho_{\alpha\alpha'} = \text{Tr}_{\mathcal{M}_n \setminus (\alpha, \alpha')}[\varrho(t)]$ is the reduced density matrix obtained by tracing out all spins of the motif except α and α' . The quantities λ_k denote the square roots of the ordered eigenvalues of the matrix $\varrho_{\alpha\alpha'} \tilde{\varrho}_{\alpha\alpha'}$, where $\tilde{\varrho}_{\alpha\alpha'}$ is the spin-flipped state [68].

Within the single-excitation subspace, the reduced density matrix takes the form

$$\varrho_{\alpha\alpha'} = \begin{pmatrix} p_{00} & 0 & 0 & 0 \\ 0 & p_{10} & \varrho_{10,01} & 0 \\ 0 & \varrho_{01,10} & p_{01} & 0 \\ 0 & 0 & 0 & 0 \end{pmatrix}, \quad (\text{S28})$$

where p_{00} is the probability of no excitation in either spin α and α' , p_{10} and p_{01} the probability of the excitation occupying α or α' , respectively, and $\varrho_{10,01}$ the corresponding coherence. This is an X-state for which the concurrence reduces to [69]

$$\mathcal{C}(\varrho_{\alpha\alpha'}) = 2 \left| \varrho_{\alpha\alpha'}^{10,01} \right| = 2 \left| \langle \sigma_{\alpha}^+ \sigma_{\alpha'}^- \rangle \right|. \quad (\text{S29})$$

The time dependence follows from the spectral decomposition of the Liouvillian, Eqs. (S2) and (S4). We isolate the contribution from the strong-dynamical-symmetry subspace spanned by $|\psi_{\pm}\rangle$, while the additional steady-state contribution $\tilde{\varrho}$ can be obtained numerically. Owing to \mathcal{C}_n symmetry, it suffices to evaluate the concurrence either between the central spin and an inner spin, or between two inner spins.

Using the definitions of $|\psi_{\pm}\rangle$ in Eq. (3) we find

$$\mathcal{C}(\varrho_{ci}) = 2 \left| \langle c | \langle i | \right| = \frac{1}{\sqrt{n}} \left| \langle \psi_+ | \varrho(0) | \psi_+ \rangle - \langle \psi_- | \varrho(0) | \psi_- \rangle - 2i \left| \langle \psi_+ | \varrho(0) | \psi_- \rangle \right| \sin(\Omega t + \varphi) \right|, \quad (\text{S30})$$

where $\langle \psi_+ | \varrho(0) | \psi_- \rangle = \left| \langle \psi_+ | \varrho(0) | \psi_- \rangle \right| e^{i\varphi}$. In general, $\tilde{\varrho}$ yields an additional (static) contribution.

Similarly,

$$\mathcal{C}(\varrho_{ij}) = 2 \left| \langle i | \langle j | \right| = \frac{1}{n} \left| \langle \psi_+ | \varrho(0) | \psi_+ \rangle + \langle \psi_- | \varrho(0) | \psi_- \rangle + 2 \left| \langle \psi_+ | \varrho(0) | \psi_- \rangle \right| \cos(\Omega t + \varphi) \right|. \quad (\text{S31})$$

For the special case that the initial state is a pure state of the form $\varrho(0) = |\psi_0\rangle \langle \psi_0|$ with

$$|\psi_0\rangle = \frac{1}{\sqrt{1+b^2}} (|\psi_+\rangle + b |\psi_-\rangle), \quad (\text{S32})$$

the concurrences are given by

$$\mathcal{C}(\varrho_{ci}) = \frac{1}{(1+b^2)\sqrt{n}} \sqrt{(1-b^2) + 4b^2 [\sin(\Omega t)]^2}, \quad (\text{S33})$$

$$\mathcal{C}(\varrho_{ij}) = \frac{1}{2n} + \frac{b}{(1+b^2)n} \cos(\Omega t). \quad (\text{S34})$$

For $b = 1$, i.e., an equal superposition of the two dynamical-symmetry eigenstates, the central–outer concurrence $\mathcal{C}(\varrho_{ci})$ oscillates between 0 and $1/\sqrt{n}$, while outer–outer concurrence $\mathcal{C}(\varrho_{ij})$ oscillates between 0 and $1/n$. The oscillation amplitudes therefore decrease with increasing n , reflecting the delocalized structure imposed by the \mathcal{C}_n symmetry of the system. Moreover, even when the oscillatory contribution vanishes, the static contribution originating from the steady state remains bounded by the same values, since rotational symmetry enforces an equal distribution of the single excitation over the inner spins.

V. LIOUVILLIAN PERTURBATION THEORY

We derive here the second-order correction to the purely imaginary Liouvillian eigenvalues associated with synchronized dynamics under coherent perturbations of the Hamiltonian. As discussed in the main text, perturbations of the dissipative rates do not alter the qualitative structure of the dynamics. We therefore consider a perturbed Hamiltonian $H + \varepsilon V$, leading to a perturbed Liouvillian $\mathcal{L} = \mathcal{L}_0 + \varepsilon \mathcal{V}$, where \mathcal{L}_0 is the Liouvillian superoperator of the unperturbed systems and $\mathcal{V}[\varrho] = -i[V, \varrho]$. We focus on the complex-conjugate pair of purely imaginary eigenvalue λ_{\pm} with eigenstates $|\varrho_{\pm}\rangle\rangle$. Since they are always a complex conjugate pair (even after perturbation due to the structure of \mathcal{L}), we specifically focus on λ_+ .

The first order equation of the (non-degenerate) perturbation theory is given by

$$\mathcal{L}_0 \left| \varrho_+^{(1)} \right\rangle\rangle + \mathcal{V} \left| \varrho_+^{(0)} \right\rangle\rangle = \lambda_+ \left| \varrho_+^{(1)} \right\rangle\rangle + \lambda_+^{(1)} \left| \varrho_+^{(0)} \right\rangle\rangle, \quad (\text{S35})$$

where $\left| \varrho_+^{(0)} \right\rangle\rangle = |\varrho_+\rangle\rangle$ of the unperturbed system. Imposing $\langle\langle \sigma_+^{(0)} | \varrho_+^{(1)} \rangle\rangle = 0$ leads to the first-order correction

$$\lambda_+^{(1)} = \langle\langle \sigma_+^{(0)} | \mathcal{V} | \varrho_+^{(0)} \rangle\rangle. \quad (\text{S36})$$

As $\mathcal{V} = -i[V, \cdot]$, the matrix element is purely imaginary. Thus, the first-order correction yields only a frequency renormalization and does not introduce decay. We therefore proceed to the second-order term.

The second order correction to the eigenvalue is given by

$$\lambda_+^{(2)} = \langle\langle \sigma_+^{(0)} | \mathcal{V} | \varrho_+^{(1)} \rangle\rangle. \quad (\text{S37})$$

To evaluate the second-order, we need to determine the first-order correction to the eigenstate. In general we can express it as

$$\left| \varrho_+^{(1)} \right\rangle\rangle = \sum_{l \neq +} c_l \left| \varrho_l^{(0)} \right\rangle\rangle. \quad (\text{S38})$$

Then from the first order Eq. (S35) we find

$$c_l = \frac{\langle\langle \sigma_l^{(0)} | \mathcal{V} | \varrho_+^{(0)} \rangle\rangle}{\lambda_+ - \lambda_l}. \quad (\text{S39})$$

The second order correction to the eigenvalue is then

$$\lambda_+^{(2)} = \sum_{l \neq +} \frac{1}{\lambda_+ - \lambda_l} \langle\langle \sigma_+^{(0)} | \mathcal{V} | \varrho_l^{(0)} \rangle\rangle \langle\langle \sigma_l^{(0)} | \mathcal{V} | \varrho_+^{(0)} \rangle\rangle. \quad (\text{S40})$$

Because λ_+ is purely imaginary while all other λ_l have strictly negative real parts, the denominator generally acquires a non-zero real component, implying that the second-order correction $\lambda_+^{(2)}$ generically acquires a real part of order ε^2 .

Thus, Hamiltonian perturbations of strength ε induce decay only at order $\mathcal{O}(\varepsilon^2)$. As long as the perturbation remains small, the imaginary part of λ_+ , and hence the synchronized oscillations, remains robust and observable over long times.